buildings

MDPI

Article

Comparison of Simulation and Measurement in a Short-Term Evaluation of the Thermal Comfort Parameters of an Office in a Low-Carbon Building

Radoslav Ponechal *, Peter Barňák and Pavol Ďurica

Department of Building Engineering and Urban Planning, Faculty of Civil Engineering, University of Zilina, Univerzitna 8215/1, 010 26 Zilina, Slovakia; barnak@uniza.sk (P.B.); pavol.durica@uniza.sk (P.Ď.)
* Correspondence: radoslav.ponechal@uniza.sk; Tel.: +421-41-513-5736

Abstract: The subject of the following analysis is the Research Centre building of the University of Zilina (RC UNIZA), which was purposely designed as a low-carbon project. The measurements of selected offices were carried out to verify how the building envelope and infill cooling system influences the indoor environment during the summer season. These measurements, along with the parameters of outdoor climate and its influence on the indoor thermal-humidity microclimate were monitored. Most of the data was then used in subsequent transient-state thermal simulation in an ESP-r program. The evaluation took two days to complete wherein an air-cooling system and ceiling radiant cooling were presented. The office during the test was not occupied and was therefore slightly cooler. Under these conditions (measured and simulated), PPD and PMV indexes were calculated during a 10 h time period with varying input parameters (metabolic heat and thermal resistance of clothing). According to the measurement and simulation, these indexes were compared. The comparison shows that the agreement depends on the chosen personal factors such as the thermal resistance of the clothing and metabolic heat. If these are chosen appropriately, then the differences between the results according to the measurement and the simulation were limited.

Keywords: thermal comfort; simulation; low-carbon; building; office; summer; overheating; window

Citation: Ponechal, R.; Barňák, P.; Ďurica, P. Comparison of Simulation and Measurement in a Short-Term Evaluation of the Thermal Comfort Parameters of an Office in a Low-Carbon Building. *Buildings* **2022**, *12*, 349. https://doi.org/10.3390/buildings12030349

Academic Editor: Tomasz Sadowski

Received: 17 January 2022
Accepted: 9 March 2022
Published: 14 March 2022

1. Introduction

Interest in studying the quality of indoor environments has been growing, especially since the second half of the last century. Although many evaluation methods of thermal comfort have been found, the predicted mean vote (PMV) and predicted percentage of dissatisfied (PPD) index are still among the most widely used [1]. An exceptional PMV/PPD model was developed by P.O. Fanger, professor at the International Center for the Indoor Environment and Energy at the Technical University of Denmark [2]. He used heat-balance equations and empirical studies to define thermal comfort model. Other institutions in various countries, such as the USA and China (as well as other countries) also took part in research on thermal comfort [3–8].

The future, under current European legislation, will belong to the construction of "low-carbon buildings", which represent a significant reduction in heating and cooling energy. However, such buildings with eminent envelope insulation are more sensitive to thermal comfort in summer, depending on the intensity of ventilation and internal heat gains [9]. This makes the evaluation of thermal comfort even more important.

Therefore, before their realization, it is good to subject the building to tests with the help of simulation tools and thus find out under what conditions overheating and discomfort in the interior can occur. Their credibility depends on many factors such as the quality of the input data, the simulation method used, and also the competence of the simulation engineer. The architect can incorporate the knowledge gained from the

simulation into the project, especially for administrative buildings, which have a special position in the evaluation of thermal comfort and productivity of work [10,11].

Many articles about the comparison of measurement and simulation have been published, some showing a high agreement [12–14] and others identifying holes in the comparison agreement [15–17]. The sensitivity analysis in [18] demonstrates that the type of window ventilation and room door opening are the most sensitive variables affecting the prediction of thermal comfort in residential buildings. ASHRAE Guideline 4-2014 [19] gives indicators for calibration, CV (RMSE) which is the coefficient of variation of root-mean-square error (RMSE), and R^2 which is the coefficient of determination (R square). It recommends that R^2 be less than 0.75 for calibrated models. However, if the simulation aims to assess the thermal comfort throughout the day (not simply the maximum air temperature), the simulation model should be calibrated according to this goal as Paliouras and the collective pointed out in their study [20]. For example, discrepancies and differences in surface temperatures, which occur even with a great deal of agreement on the consistency of the simulation measurement results, can induce uncertainties up to 0.5–1.0 points on the thermal sensation scale [21,22].

In any case, this was determined on the basis of theoretical calculations of the fictitious indoor environment. It is not well known how this will be reflected in a specific office. In a real operation, the conditions of the indoor environment are not the same during the day. In particular, the temperature of the dazzled surfaces varies considerably. Therefore, the thermal comfort estimation may deviate during the day. There is a concern that this deviation might confuse the building category according EN 16798 standard [23]. All of this can be verified by comparing measurements and simulations in the building during operation.

2. Materials and Methods

2.1. Case Study Building Charakteristics

As already mentioned, low-carbon buildings are now preferred. As a result, we chose the Research Centre of the University of Žilina building (RC UNIZA) (Figure 1), which was designed and built in such a standard [24] (Table 1). RC UNIZA serves as an experimental and educational stock in the field of energy performance and energy efficiency of buildings. It has five floors above ground and one floor below ground. The envelope construction consists of a reinforced concrete skeleton with a 380 mm thick porous concrete block masonry infill. The external insulation layer was made of 200 mm thick mineral wool boards. The windows on the Research Centre building have plastic six-chamber frames and triple glazing with a heat transfer coefficient Ug = 0.6 ($W/(m^2\ K)$) and total solar energy transmittance g = 0.5 (-). Exterior blinds are installed on the windows, which can be manually controlled from each room or automatically through an automatic control system which connects to the central building control system. The main heating system is an underfloor radiant system. A radiant cooling system is installed in the plasterboard ceilings. The cooling system is divided into individual zones per floor and is connected to a control system that records the room temperature, the amount of CO_2 in the room, the air flow rate, etc.

Table 1. Summary table of building passive house characteristics.

Quantity	Requirements [24]	Value
Opaque construction mean U-value	$\leq$0.15 $W/(m^2\ K)$	0.145 $W/(m^2\ K)$
Windows U_w/g	$\leq$0.8 $W/(m^2\ K)/\geq$ 0.5 (-)	0.76 $W/(m^2\ K)$/0.5 (-)
Airtightness	0.6 h^{-1}	0.49 h^{-1}
Space heating energy demand	15 kWh/m^2	13.2 kWh/m^2

(**a**) (**b**)

Figure 1. (**a**) West-side view of the Research Center building with red arrow indicating measured office; (**b**) floor-plan with red rectangle indicates measured office.

A small amount of energy required for operation is produced mainly from renewable sources. The energy is produced by a water-to-water heat pump system, while the energy to produce heat and cold is obtained from deep boreholes. The building generates electricity using photovoltaics (PV), which can also be used by a heat pump.

2.2. Office Room Charakteristics

We chose an office in the RC UNIZA building, located on the second floor and facing west, as the experimental site (Figure 2).

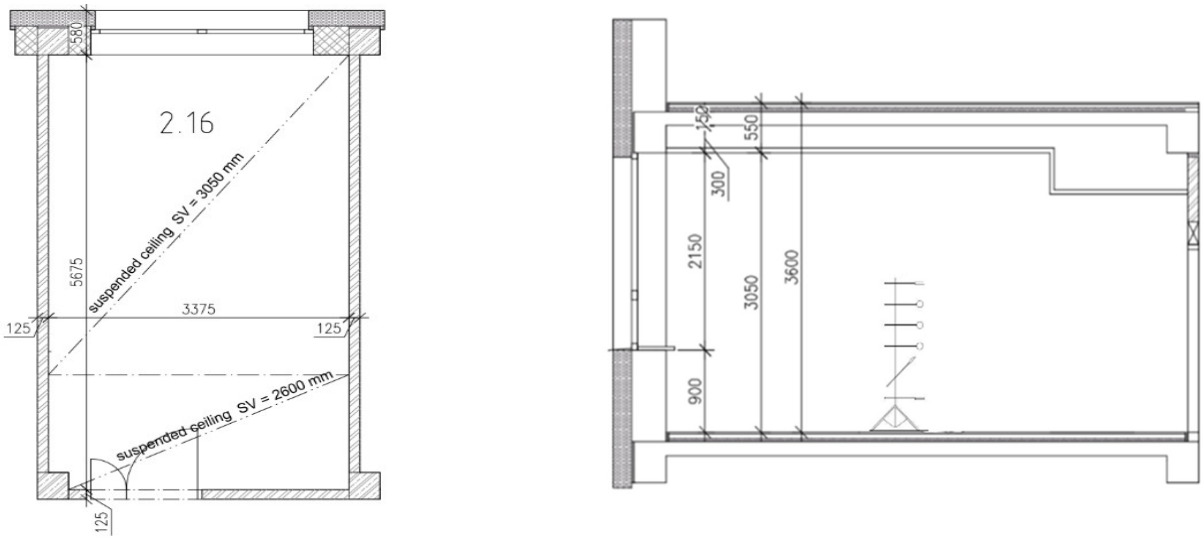

(**a**) (**b**)

Figure 2. (**a**) Floor plan of the office, and (**b**) the section of the office.

The internal partition walls were also made of 125 and 150 mm thick aerated concrete blocks. The ceiling slabs are 150 mm thick reinforced concrete insulated with a 30 mm thick system board with step insulation and a total slab thickness of 50 mm. Although there are

exterior blinds installed on the office window. They were pulled out all of the time during the two-week measurement period to verify overheating.

2.3. Measuring Methods and Instrumentation

Although temperatures were measured and simulated, the final output of the indoor environment assessment is the PMV and PPD indices of thermal comfort. To evaluate these indices, the following data must be measured: air temperature, mean radiant temperature, air velocity and humidity. During the biweekly measurements, these values were recorded and then evaluated. The mean radiant temperature was calculated from the measured data.

Various probes and thermocouples, connected to a measuring panel, were deployed for measurements inside the office (Figure 3)(Table 2). The ComfortSense device from Dantec Dynamic [25] was equipped with the following probes:

- A probe for measuring relative humidity—accuracy in temperature range 10–30 °C is ±1.5%;
- Resistance wire probes for measuring air velocity- accuracy ±2% in range 0.05–1 m/s;
- Air temperature sensors using a thermocouple K (NiCr-Ni)- accuracy was ±0.2 K in range of 0 to +45 °C;
- Probe for measuring the operative temperature (not used).

(**a**) (**b**) (**c**)

Figure 3. Indoor instrumentation: (**a**) ComfortSence measuring device, (**b**) globe temperature probe, and (**c**) Pt100 sensors for window surface temperature measurement.

Table 2. Summary table of the instrumentation.

Sensor	Location in the Office
Relative humidity probe	in the centre, at height 1.5 m above the floor
Four drauht probes for measuring air velocity and temperature	in the centre, at height 0.15, 0.9, 1.1 and 1.3 m above the floor
Globe temperature sensor	in the centre, at height 1.1 m above the floor
Surface temperature sensors	in the centre of each surface

The measuring elements of the device meet the standards EN 13 182, ISO 7726 and ISO 7730 [26–28]. A black globe temperature sensor with a 150 mm diameter copper sphere mounted on a stand 1.1 m above the floor was also used with accuracy ±0.5 K over a temperature range of 0 to +50 °C. Pt100 thermocouples were used on the ceiling, floor, and window structure (glazing and frames) to measure surface temperatures with accuracy ±0.3 K at 0 °C. The surface temperature on the partitions was not measured. On the glazing, shading of the thermocouple from the exterior side from direct sunlight was ensured. Data

were recorded at 5-min intervals. The measured values of air velocity ranged from 0.01 m/s to 0.09 m/s. The measured relative air humidity ranged from 50% to 60% RH.

2.4. Meteorological Data

It is necessary to enter the correct climatic data into the simulation. A weather station located on the roof near the Research Centre building was used to measure outdoor climatic parameters (Figure 4). The outdoor air temperature, solar radiation intensity, and air velocity were measured using this weather station.

Figure 4. Weather station on the building rooftop near the Research Center from which data on the external environment was used [29].

2.5. Simulation Model

Since it was only possible to measure the operative temperature in the centre of the room, it was necessary to use a simulation tool for a comprehensive assessment in the space. The ESP-r program developed as a research tool [30] which allows the mean radiant temperature calculation at sensor position. When it comes to simulating the heat capacity, it is one of the most accurate simulation tools using a finite volume approach for solving a set of conservation equations. As can be seen in (Figure 5) the room was modelled with all of the structures and equipment that can affect the indoor temperature. Also, a tree obstacle in the form of a wall was modeled, since there is a forest belt near the building and this may affect the impact of solar radiation on the building. Before carrying out the simulation, the input data was completed (construction and material details, boundary conditions and air flow schedules, etc.). All boundary conditions on the interior surfaces except on the facade were adiabatic. The air flow schedules were divided into infiltration and ventilation. Infiltration corresponds to the amount of air coming from the ambient through the windows, and it was chosen according the air-tightness of the building (0.03 1/h). Internal heat gains from the instrumentation and computer alone of 150 W were entered into the model and split between the radiant component (20%) and the convective flow (80%). The possibility of human occupancy was not taken into account (the room was empty during the measurements).

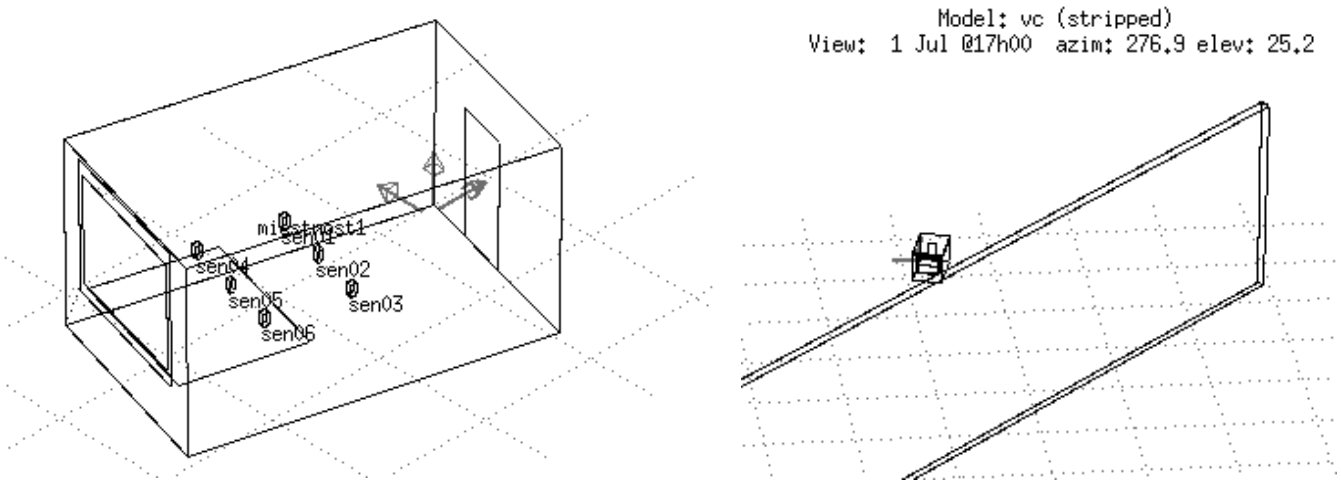

Figure 5. On the left a simplified simulation model of the office in ESP-r program with six MRT sensors, on the right a view from the sun on the office and an obstacle (row of trees) in ESP-r program.

During the measurement period (28 June 2020–4 July 2020) two types of cooling systems were used to cool the room had to be included in the simulation model. Intensive cooling was provided on 29 and 30 June by the air handling unit in the early morning hours before the start of working hours. This was simulated by a fully convective cooling system. All cooling power was efficiently transferred to the air in the office. Cooling was provided by a ground borehole and ran throughout the morning. As the temperature of the outside air that was drawn into the air handling unit rises and the eco-cooling system has its capacity, for operational reasons it was switched off after 16:00 and intensive cooling was stopped to recharge the borehole for the next day's cooling cycle (Table 3). Mixed flow convection model using Fisher correlations [31] for heat transfer determination was used.

Table 3. Simulation model setup description.

29–30 June (Air-Conditioner Cooling)			**1–2 July (Radiant Cooling)**		
ventilation source air temperature		indoor environment control law: free-floating	ceiling surface temperature		ventilation source: outdoor air indoor environment control law: free-floating
time period:	setup		time period:	setup	
0:00–7:00	18 °C		0:00–7:00	25 °C	
7:00–12:00	17 °C		7:00–9:00	24 °C	
12:00–16:00	19 °C		9:00–21:00	18 °C	
16:00–19:00	26 °C		21:00–24:00	23 °C	
19:00–22:00	22 °C				
22:00–24:00	19 °C				

The second type of cooling, ceiling radiant cooling, was launched on 1.7. This cooling system is not connected to renewable sources but conventionally with a chiller on the roof of the building (this cooling has a higher capacity and allows for higher cooling performance). This cooling system is secondary and is used only on very hot days. Otherwise, the building is cooled throughout the summer by air conditioning with cooling pumped from a ground borehole. The fresh air supply to the room was fixed to the intensity of air change n = 0.8 1/h in the simulation program. The simulation was performed for four days (plus seven start-up or conditioning days) at a time-step of 5 min. The outdoor climatic boundary condition was fitted in the simulation based on measurements from the meteorological station on the University campus. The record of the main outdoor climatic conditions during the three hot days is shown in (Figure 6).

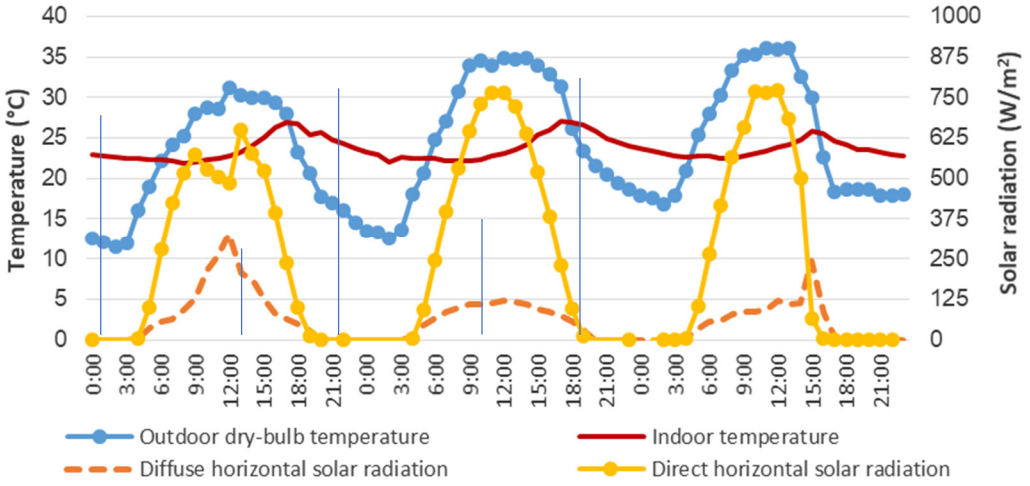

Figure 6. Measured climatic parameters and indoor temperature at 29.6 to 1.7.

It can be observed that the temperature had been rising from day-to-day. It reached its maximum on 1.7. When the highest temperature during the two-week measurement period was measured at 36.8 °C and the highest direct solar radiation intensity reached 773 W/m^2.

Although many inaccuracies such as outdoor air temperature, solar radiation, space dimensions and physical properties of materials have been eliminated, there were still some significant inaccuracies such as the distribution of incident solar gains (fraction via surface to air), convective heat transfer coefficients, air temperature stratification and the air temperature in the surrounding offices (which was not measured).

2.6. Temperature Waveforms Comparison between Measurement and Simulation

Figures 7–12 shows a comparison of the measured quantities with the same quantities from the simulation. On 29 June and 30 June room cooling was provided by an air-conditioning connected to a ground borehole. As can be seen from the waveforms, the air temperatures in the simulation are close to the measured values for this type of cooling (Figure 7). In Figure 7, we can observe the good coincidence of the all-day temperature traces from the measured values and the simulation that was achieved. It is evident that 29.6 and 30.6. temperatures reach their maxima at the same time of the day, namely at 17:30 h. On these days the indoor temperature at this time rose to 27.1 and 27.4 °C, respectively.

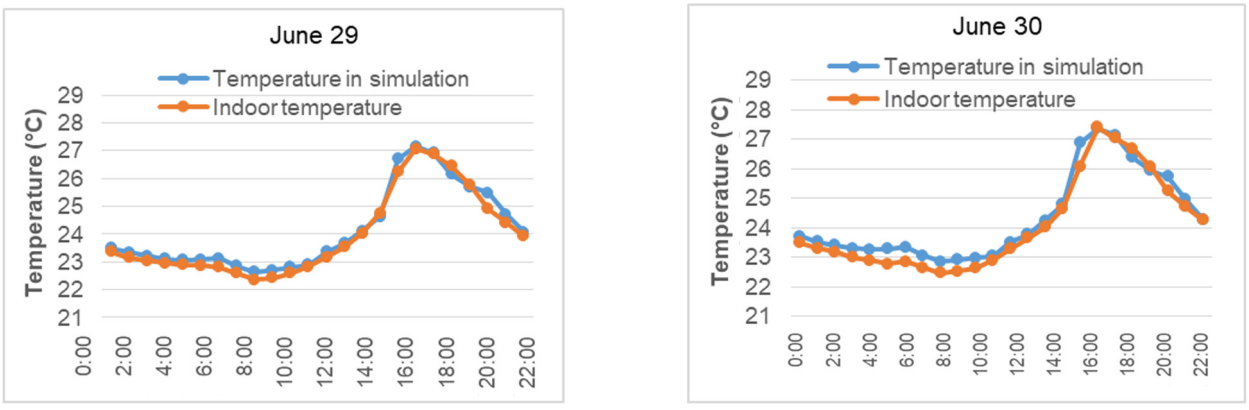

(**a**) (**b**)

Figure 7. Comparison of the all-day course of internal temperatures from the measured values from the simulation: (**a**) for 29 June, (**b**) for 30 June.

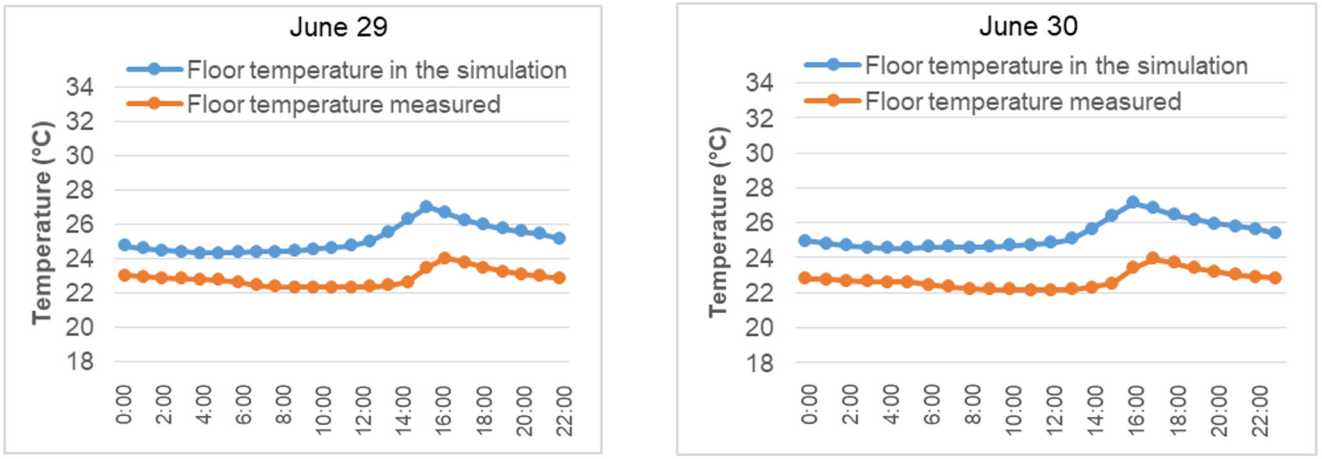

(**a**) (**b**)

Figure 8. Comparison of all-day temperature profiles on the floor from measured values with simulation: (**a**) for 29 June, (**b**) for 30 June.

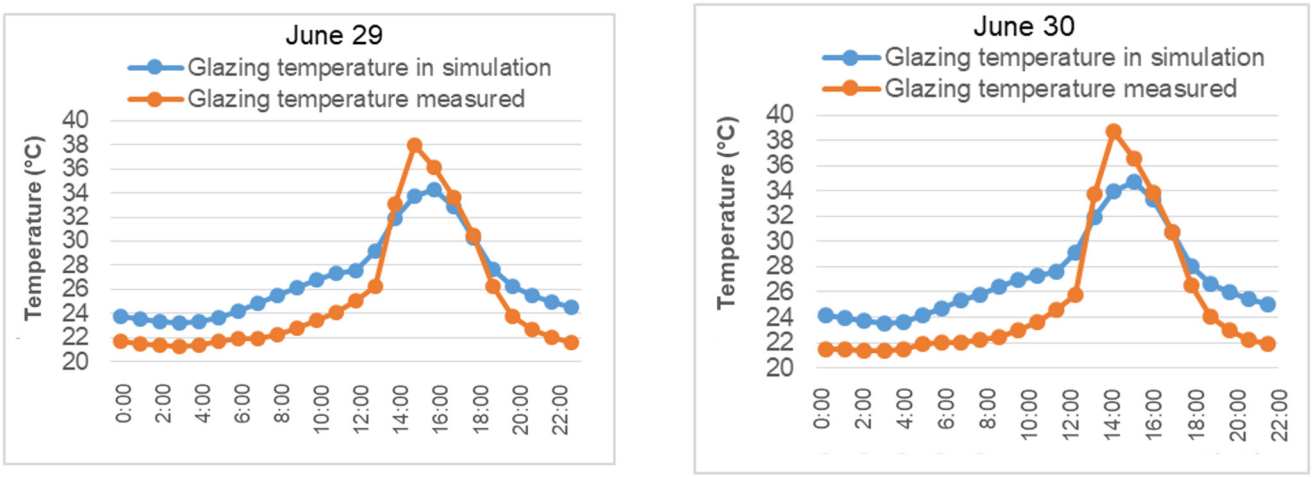

(**a**) (**b**)

Figure 9. Comparison of all-day surface temperature profiles measured in a centre of the window glazing with simulation results: (**a**) for 29 June, (**b**) for 30 June.

For the floor surface temperatures, there were some variations caused by the air temperature stratification over the room height. Figure 8 shows a comparison of floor temperatures from the simulation and from the measured values. It is again clear that the waveforms during 29.6. and 30.6. are identical, differing only in their maxima. On 29 June, we managed to reconcile the time when the measured value and the value of the simulation reached their maximum at the same time at 17:30. The measured value was 24.0 °C and on the contrary the value from the simulation reached up to 26.7 °C. On 30 June, the waveforms also coincide, even if the measured value is lower than the simulated one. We reached the highest value in the simulation one hour earlier than the previous day, at 4:30 p.m. and reached a value of 27.2 °C. The measured value reached its maximum at 5:30 p.m. and had a height of 23.9 °C.

In the following figures, we compared the effect of solar radiation on the window structure and the temperatures that were captured on the glazing and frame surfaces. We observed that the measured waveforms during 29 June and 30 June were identical in this case, but the measured and simulated surface temperatures on the glazing (Figure 9) and on the frame (Figure 10) are less consistent. On both days, the maximum temperatures in

the middle of the glazing were measured at the same hour (15:30). The temperature rose to 38.0 °C and 38.7 °C, respectively. In the simulation, we could not reach these values and the maxima were reached one hour later, at 16:30. Temperatures in the simulation rose to 34.3 °C and 34.7 °C, respectively.

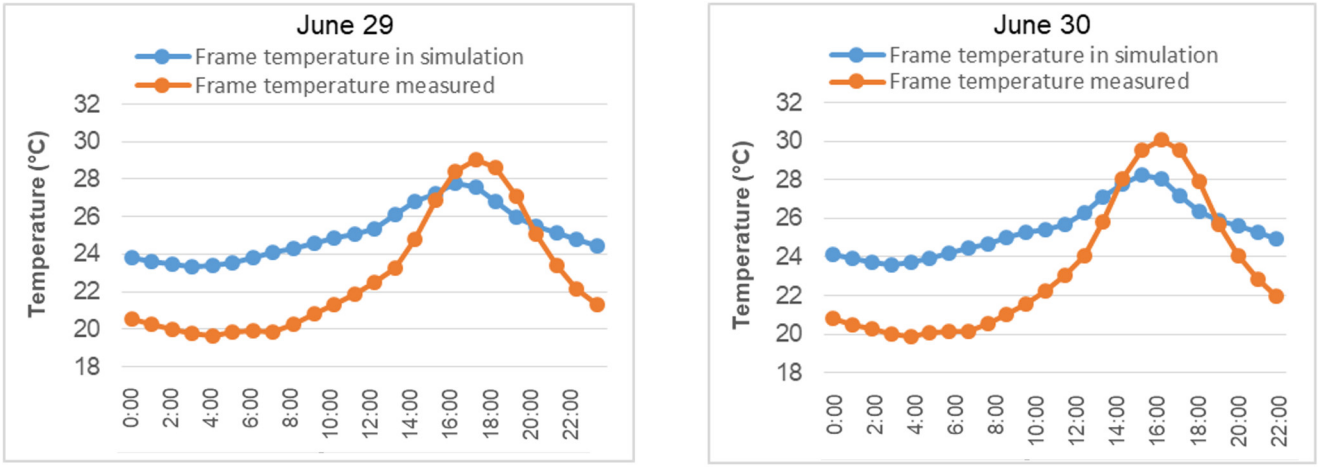

(**a**) (**b**)

Figure 10. Comparison of all-day surface temperature profiles on a window frame from measured values with simulation: (**a**) for 29 June, (**b**) for 30 June.

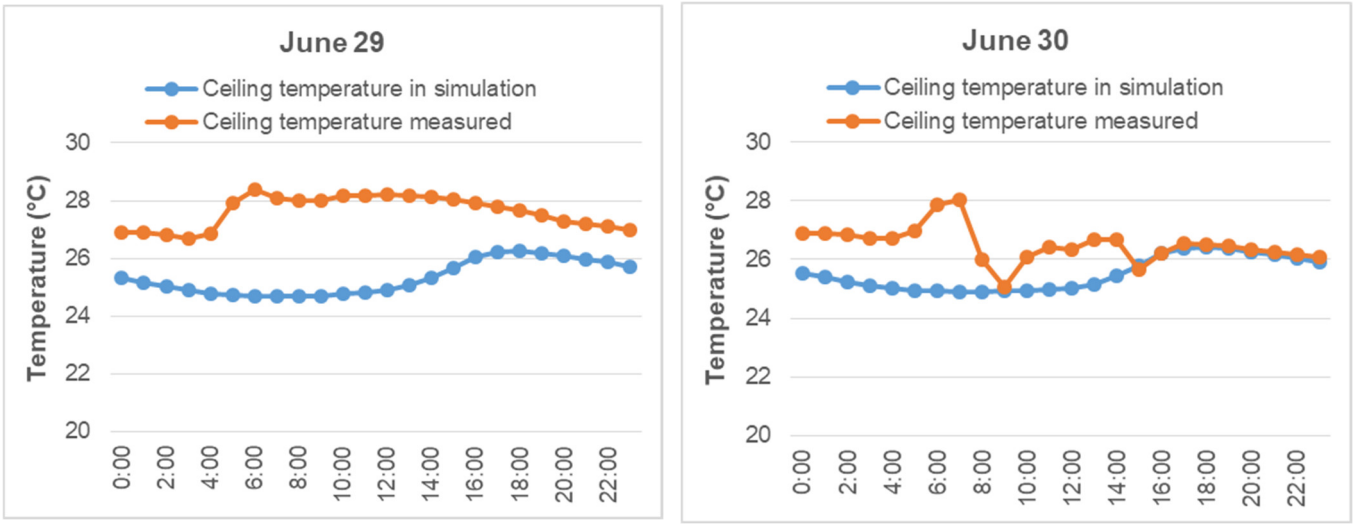

(**a**) (**b**)

Figure 11. Comparison of all-day surface temperature profiles on a window structure from measured values with simulation: (**a**) for 29 June, (**b**) for 30 June.

The temperature measured by the thermocouples is lower most of the time than in the simulation, which may be due to the ventilation outlet setup at the ceiling where the cool air is more ventilated by the window structure. The difference in the maximum temperature may be due to the sunlight hitting the thermocouple, which heats up more, even though it has been shielded a little by taping over a small area of the glazing with tape from the exterior.

Figure 10 evaluates the temperature at the frame and the effect of solar radiation on this part of the window structure. It can be seen in this figure that the waveforms are identical. The temperatures in the simulation were more stabile than measured. On 29 and

30 June, the frame temperatures from the measured ones climbed to 29.0 and 30.1 °C after both days. Those temperatures were measured at the same time at 17:30. The highest values were reached one hour earlier at 16:30 in the simulation and the temperatures were lower (27.8 and 28.3 °C).

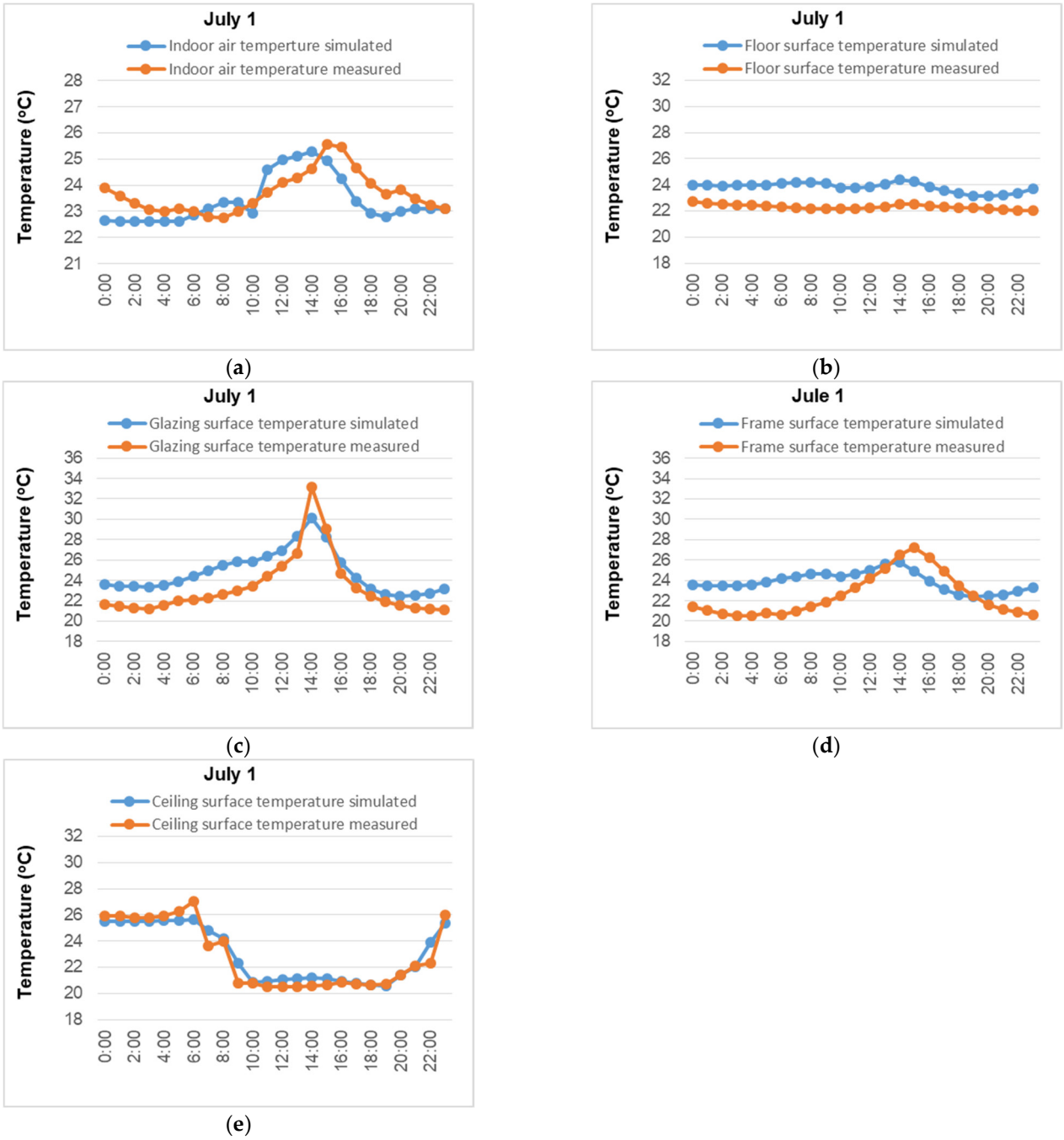

Figure 12. Comparison of all-day courses of indoor air and surface temperatures: (**a**) indoor air temperature, (**b**) floor surface temperatures, (**c**) surface temperatures on glazing, (**d**) surface temperatures on the window frame, and (**e**) surface temperatures on the ceiling.

It is interesting to look at the comparison of surface temperature waveforms on ceilings in Figure 11. The simulated waveforms were approximately the same on both days, while the measured waveforms were different. The different course on 30 June is probably related to the gradual transition to radiant ceiling cooling. At the end of the day, there was even

an apparent agreement between the measurement and the simulation. The priority in the simulation became the agreement in the surface temperature of the ceiling.

On 1 July, the cooling system in the building and the room was changed. The air-conditioning was no longer used for cooling, but radiant cooling from the ceiling was started. This is clearly visible from the course of the ceiling surface temperatures. This day was very warm, but it was cloudy in the afternoon. Figure 12 shows all courses of measured temperatures in comparison with the simulation.

From the all-day course of air temperatures in the office is clear that this type of cooling has a higher power, which strongly affects the air temperature. Achieving agreement between measurement and simulation in the air temperature was more difficult in this case. In contrast to the previous two days, there were larger discrepancies in the measured values and simulation courses. It is quite probable that this was caused by a change in the office ventilation. On this day, the measured value of the indoor air temperature reached a maximum at 17:30, with a value of 25.6 °C, and in the simulation it reached its maximum at 14:30 (namely a value of 25.3 °C).

As with the comparison of indoor air temperatures and the comparison of floor temperatures, there is a discrepancy between the simulation processes and the measured values. The simulated surface temperature was still higher than previously measured. The discrepancy between the curves can be caused by a change in the cooling system. In contrast to the previous two days, the daily highest recorded value on the floor at 15:30 was 22.4 °C; in the simulation the highest value was recorded at 14:30 (which was 24.4 °C).

When evaluating and comparing the glazing surface temperature, the courses of the measured values are relatively identical from the simulations, although there were also smaller deviations. The measured glazing temperature was the highest at 14:30, namely 33.2 °C. By the simulation, we reached the maximum also at the same hour, but the temperature was slightly lower, namely 30.2 °C.

When comparing the temperatures on the frame, the curves from the measured values and the simulation also do not match. The temperature on the frame on this day rose at the highest at 15:30, to a value of 27.2 °C. In the simulation, we reached this highest value an hour earlier, namely 25.8 °C.

3. Results and Discussion

3.1. Evaluation of Thermal Comfort by Fanger Indices

To evaluate thermal comfort by Fanger indexes, the web-based CBE Thermal Comfort Tool complies with EN 16798 was used [32]. Its advantage is that the software calculates the relative air speed for the higher metabolic rates automatically. In Figures 13–15, PMV and PPD indices were evaluated from the measured and simulated values concerning 10-h working hours (7:00–17:00). For better evaluation, we used different values of clothing and metabolism that are recommended by the standard ISO 7730. Metabolic values varied in the higher level: 1.2 met (sitting) and 1.4 met (standing) and also clothing values in the range of 0.5–0.61 clo, as each person has a different metabolism and also dresses differently [2,33]. Higher values of metabolism and thermal resistance of clothing were chosen due to the slightly colder measured thermal environment in the west-oriented office. This is due to an improper cooling system setup, which is probably a minor disadvantage of this study. It should also be noted that the air velocity was entered according to the measurement. The simulations did not have such a result.

Figure 13 evaluates the PMV and PPD indices on 30 June and 1 July. The evaluation took place over a 24-h or 10-h time intervals before the start of working hours, which is shown in the red rectangle, the room was intensively ventilated. This affected the results of the thermal comfort in the morning. In cases, when the values of metabolism and thermal resistance of clothing are lower, people in the room felt cold (1.2 met and 0.5 clo). The situation does not improve until the end of working hours. Then the room temperature rises.

Although the local maxima and minima of PMV index coincide, there were large differences in the perception of thermal comfort according to simulations and measurements. These differences were on 1 July with radiant cooling less than 30 June with air-conditioned cooling.

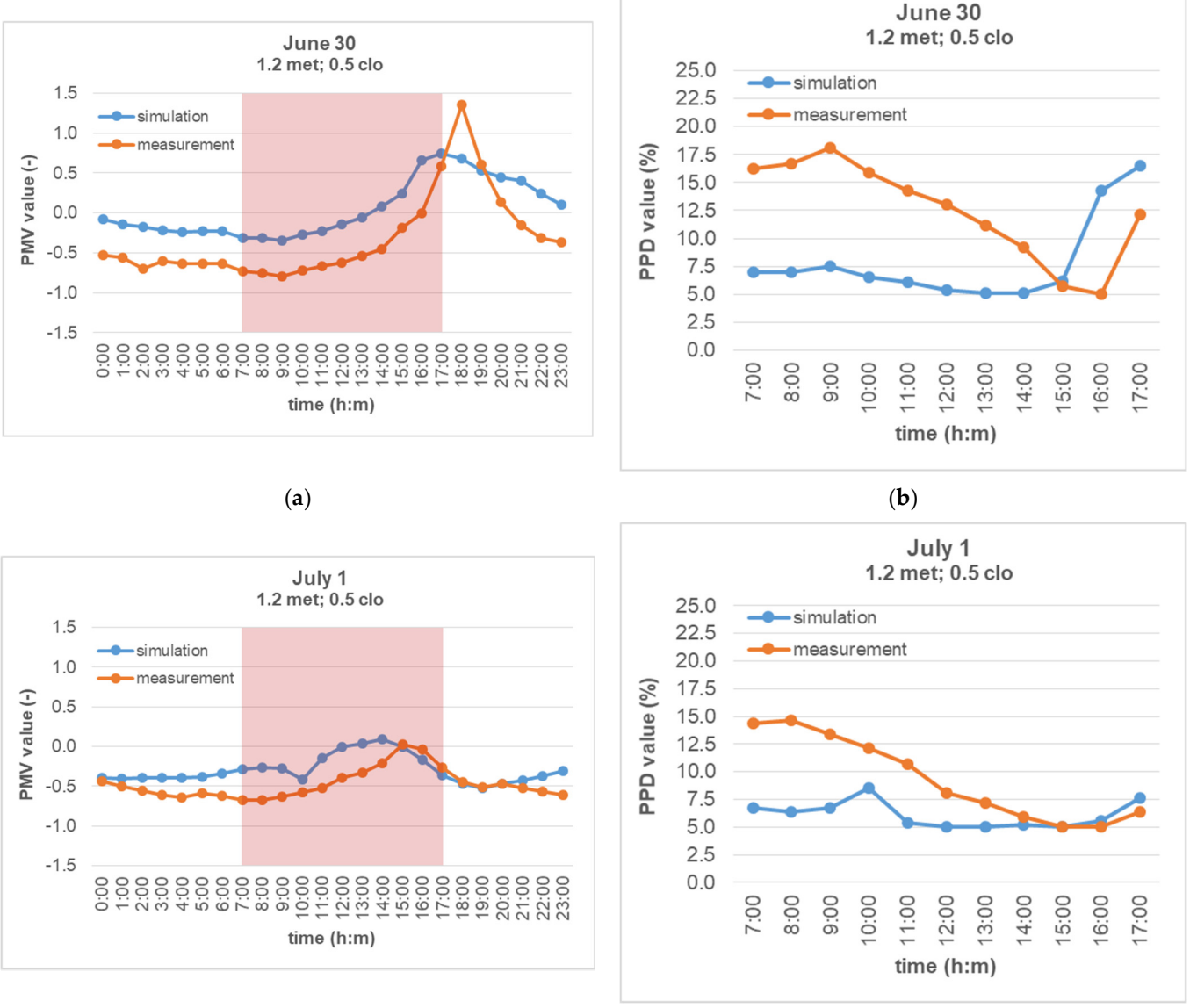

Figure 13. Evaluation of PMV and PPD indices using the typical values of metabolism (1.2 met) and clothing resistance (0.5 clo): (**a**) PMV on 30 June, (**b**) PPD on 30 June, (**c**) PMV on 1 July, (**d**) PPD on 1 July.

In Figure 14 we also evaluated the PMV and PPD indices with the high metabolic rate (1.4 met) so they could feel more comfortable. This corresponds to a person in standing slight activity. There were large differences in the perception of thermal comfort according to simulations and measurements also in this case. While according to the simulation the building was classified by environmental indoor quality (EIQ) Category I, according to the measurement it should have been classified as EIQ Category II, sometimes even category III. On the afternoon of 30 June, it was turned, but there was created the same inaccuracy changing the category of the building. On 1 July, the same thing happened on a smaller scale.

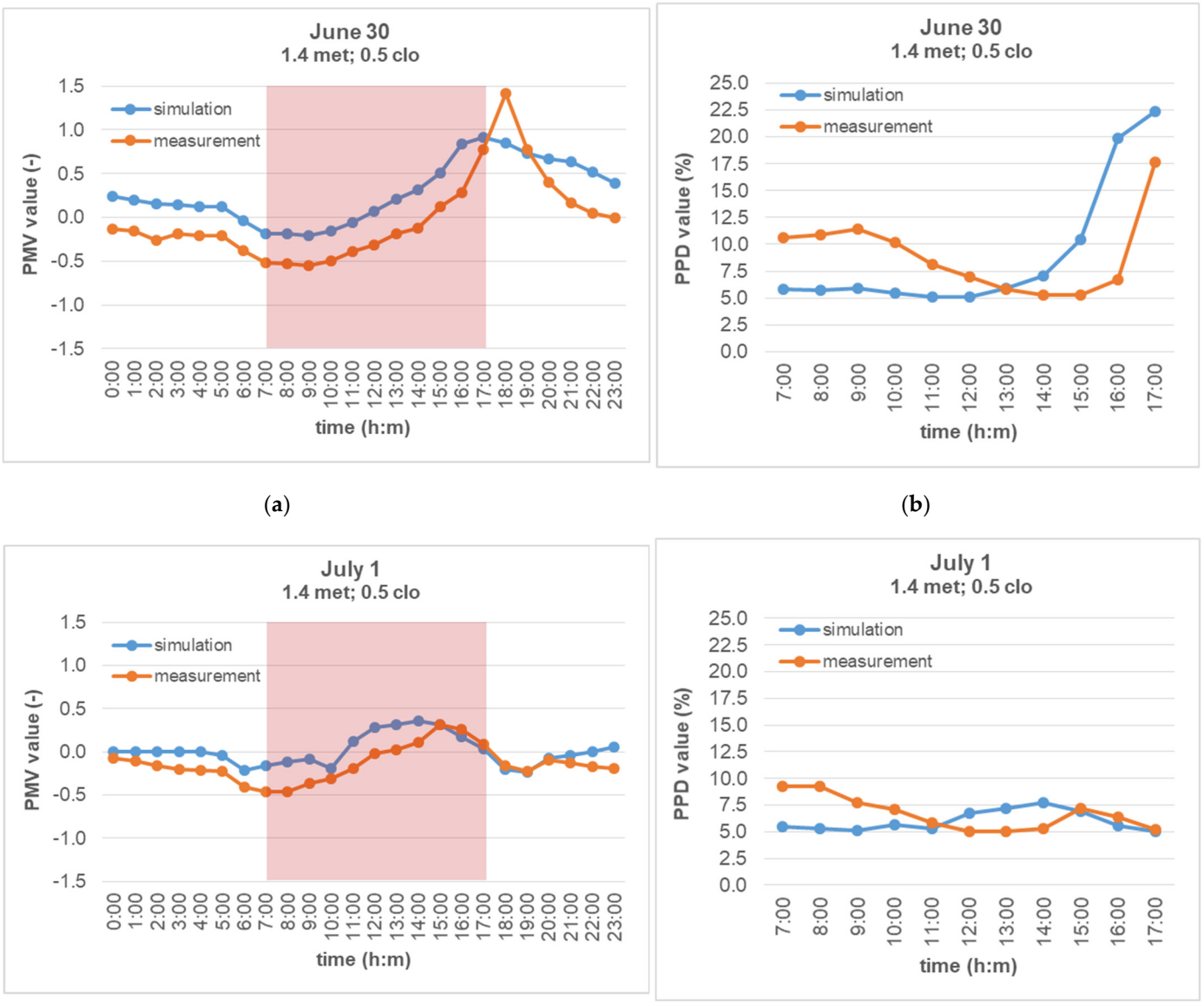

Figure 14. Evaluation of PMV and PPD indices using the highest values of metabolism (1.4 met) and clothing resistance (0.5 clo): (**a**) PMV on 30 June, (**b**) PPD on 30 June, (**c**) PMV on 1 July, (**d**) PPD on 1 July.

Figure 15 documents the results with the next combination of the metabolism (1.2 met) and higher thermal resistance of clothing (0.61 clo). It supposed to be a man dressed with trousers and a long-sleeved shirt. It is clear from the pictures that PMV index reached optimal values in the middle of the working hours. On 30 June the higher thermal resistance of clothing in was stressful in the evening. There were no problems such as this on 1 July. There was even a quite conformity between the simulated and measured PMV/PPD indices. This was expected due to the colder thermal environment in the office. According to the simulation results, it seemed that the building could be classified in EIQ Category I, but the measurement was refuted it and dropped the building into EIQ Category II.

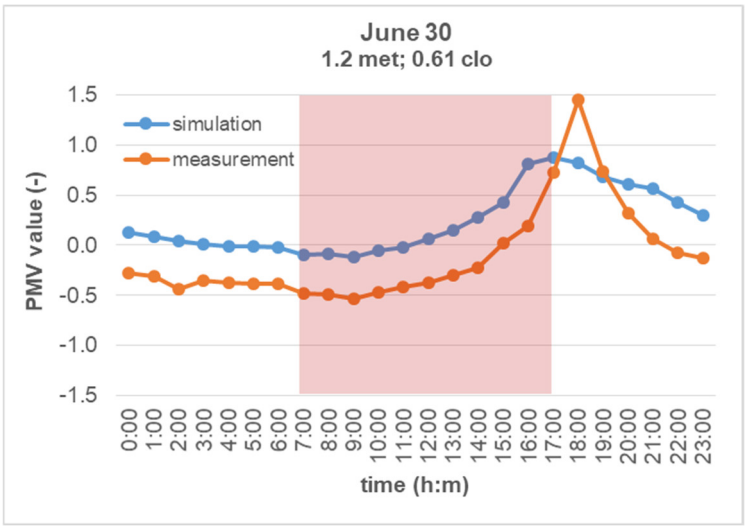

(**a**)

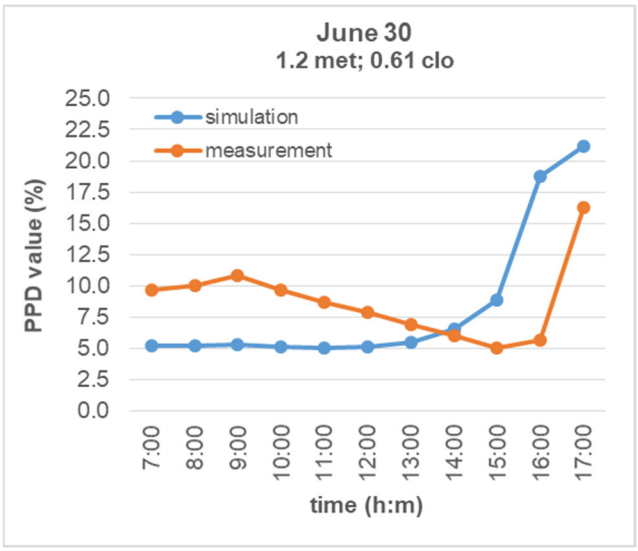

(**b**)

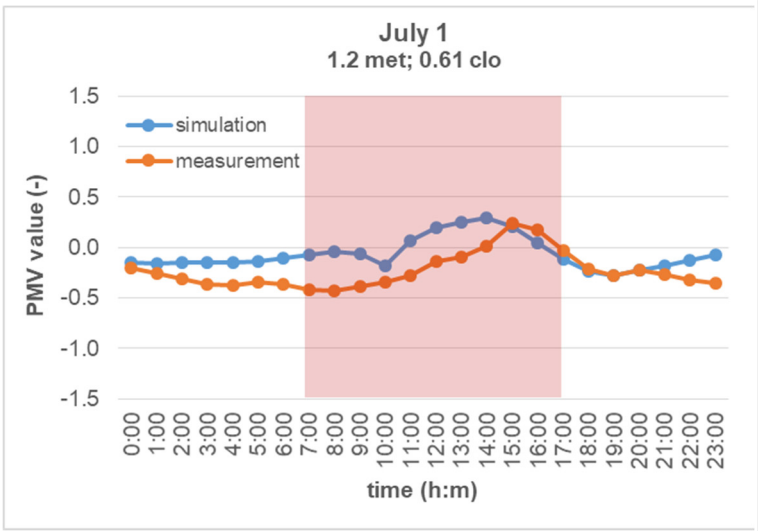

(**c**)

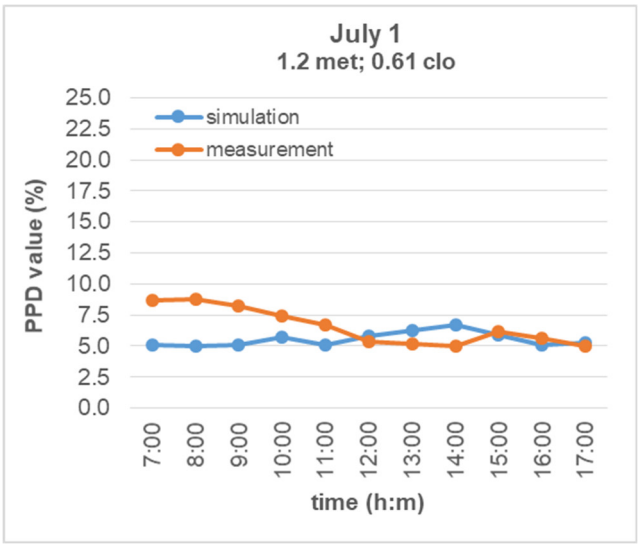

(**d**)

Figure 15. Evaluation of PMV and PPD indices using typical values of metabolism (1.2 met) and clothing resistance (0.61 clo): (**a**) PMV on 30 June, (**b**) PPD on 30 June, (**c**) PMV on 1 July, (**d**) PPD on 1 July.

3.2. MRT Sensor Position vs. Fanger Indices

The following figures show the evaluation of PPD indices from the simulation by using mean radiant temperature (MRT) sensor in the ESP-r simulation program. The indices were evaluated for six MRT sensor positions in office (see Figure 5). Three sensors near the window gave approximately the same results. While the three sensors in the center of the offset also provided almost the same MRT value. The biggest difference was in the distance of the sensor from the facade. This difference was 1 July with a radiant cooling system less than on 30 June with air-conditioning cooling (Figure 16). It could be assumed that the radiative system will provide more homogenous conditioning to the space. To evaluate the indices in these graphs, we used the commonly-used values of metabolism (1.2 met) and thermal resistance of clothing (0.5 clo). Under these conditions, the workers feel slightly cold in the morning and their position in the room does not change much. In the afternoon on 30 June, the window warmed up from direct sunlight and the difference in thermal

sensation by position was greater. We observed this at the end of common working hours. The working hours are marked in the figure with a colored square (Figure 17).

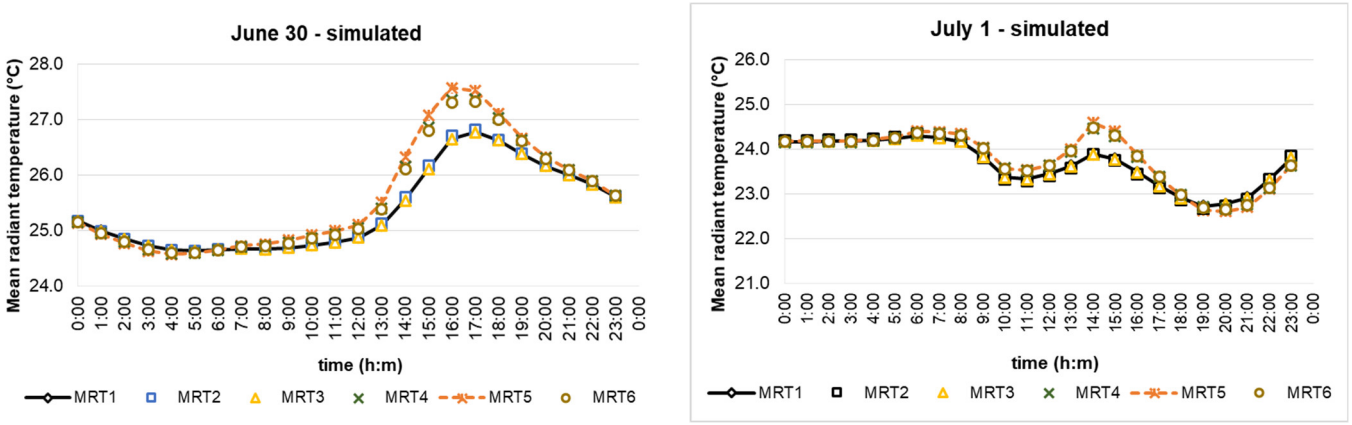

(**a**) (**b**)

Figure 16. Evaluation of PPD indices from the simulation at different positions in the room (sen01–06): (**a**) for 30 June, (**b**) for 1 July.

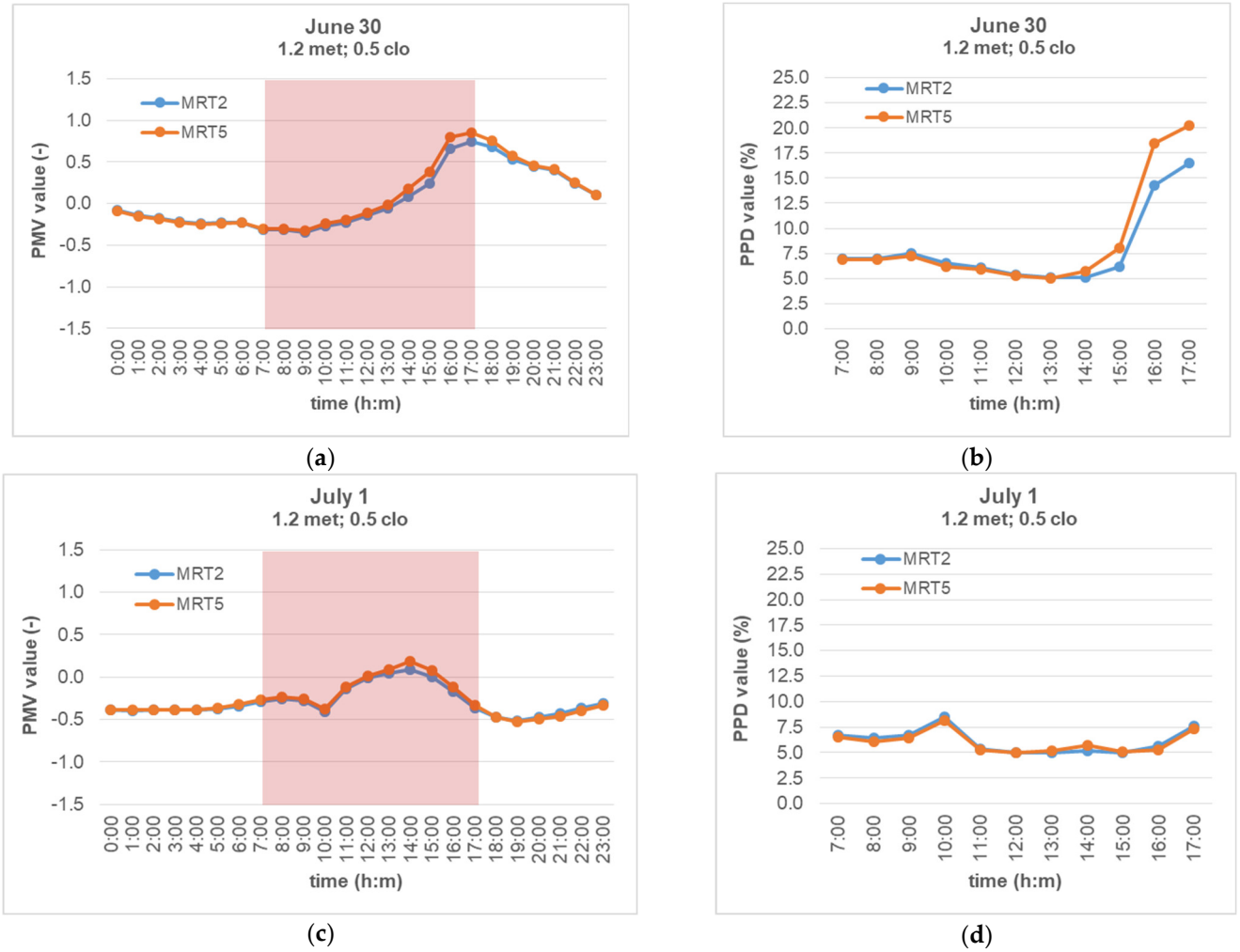

(**a**) (**b**)

(**c**) (**d**)

Figure 17. Evaluation of PPD indices from the simulation at different positions of MRT sensors in the room (MRT 5 was the closest to the window and MRT 2 was in the centre of the office): (**a**) PMV on 30 June, (**b**) PPD on 30 June, (**c**) PMV on 1 July, (**d**) PPD on 1 July.

3.3. Temperature Differences and PMV Index

The dependence of the differences in the measured and simulated temperature on the value of PMV indices can be seen in the combined graphs in Figure 18. You can clearly see the big difference that arose between the simulated and the measured MRT value. Although it increased to 4 K during the day, the difference in the PMV index changed little and remained at about 0.5 points. This was due to the fact that the difference in air temperature over lunch on 30 June dropped to almost zero. The simulation was calibrated to ensure a good agreement in the simulated and measured maximum air temperature. The difference in MRT was smaller on 1 July, but the difference in air temperature increased. The simulation was calibrated to ensure a good agreement in the ceiling surface temperature on this day.

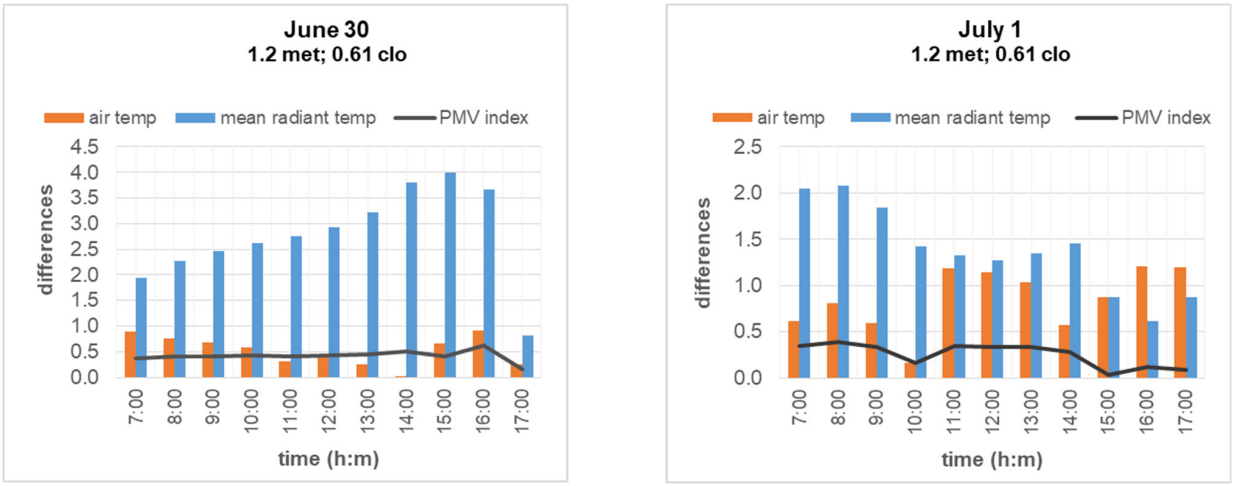

(**a**) (**b**)

Figure 18. Comparison of PPD indices and temperature differences between measurement and simulation: (**a**) for 30 June, (**b**) for 1 July.

Differences between measurement and simulation were also quantified using statistical variables. An overview of these results is given in Table 4. As expected, there is a relatively big value of the coefficient of variation for mean radiant temperature on 30 June. The captured 12.0% of CV (RMSE) is much more than the 5% needed for a good agreement. Better results were achieved for 1 July. The CV (RMSE) for mean radiant temperature was 6.0% and the root-mean-square error for PMV index decreased from 0.43 point to 0.28 points. However, this is still a big deviation in terms of the values that cause the building to be recategorized according to the EIQ assessment. Thus, the biggest problem is not the correct simulation of the indoor air temperature but the mean radiant temperature agreement. The resulting evaluation of thermal comfort will be the most dependent on the calibration of this quantity. This cannot be carried out without a detailed measurement of all surface temperatures. Therefore, it will be more difficult to correctly predict the quality of the indoor thermal environment of buildings than its energy consumption.

Table 4. Summary table of statistical analysis of differences between measurement and simulation.

Variable	RMSE	CV (RMSE)
Indoor air temperature—30 June	0.59	2.5%
Mean radiant temperature—30 June	2.91	12.0%
PMV index—30 June	0.43	-
Indoor air temperature—1 July	0.91	3.8%
Mean radiant temperature—1 July	1.4	6.0%
PMV index—1 July	0.28	-

3.4. Accumulated PPD Index

In addition, we supplement the comparison of measurement and simulation results with the accumulated PPD index indicator (Figure 19). With unsuitable clothing and low activity, the differences in the summary thermal sensation were evidently large. With the suitable clothes and activity, they were significantly smaller. The simulation can be then considered more accurate. This observation was independent of how the office was cooled. The comparison is distorted around the neutral feeling. The PPD index is the same, although the group of people were a little cold according to the measurement and a little warm according to the simulation. Due to this fact, the differences in the PPD index are smaller than in the PMV index.

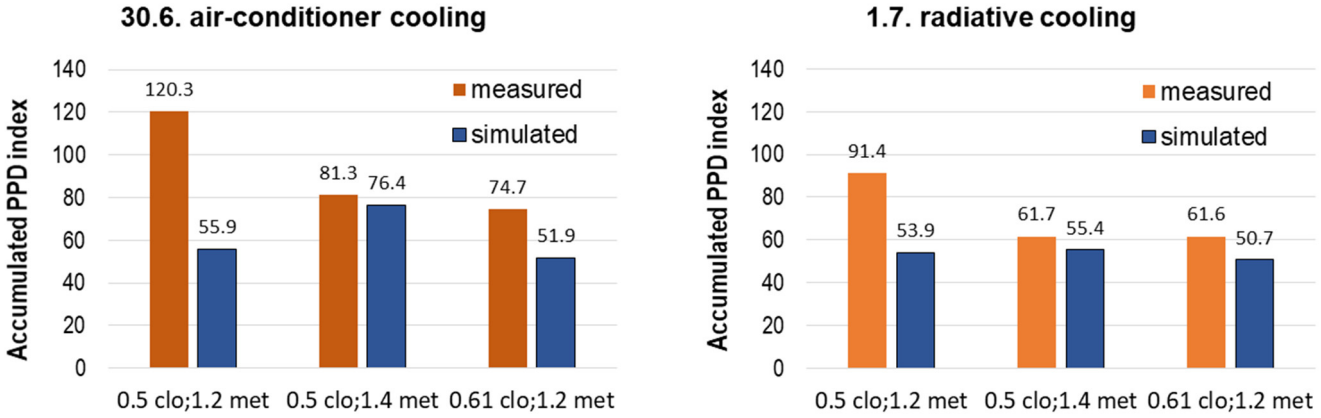

Figure 19. Comparison of cumulative PPD indices calculated from measured data and from simulated data: (**a**) for 30 June, (**b**) for 1 July.

4. Conclusions

The aim of the paper was not to compare two cooling systems in the same office as in other papers. The intention was to compare the measured quantities with the same quantities from simulation and to tune the simulation model in the ESP-r tool to obtain identical waveforms. Among other things, the work aimed to find and compare PMV and PPD indices from measured and simulated values when combining different values of thermal resistance of clothing and human metabolism.

As it turns out, it is not possible to evaluate the accuracy of the simulation in the summer only by the air temperature profiles between the measurement and the simulation comparison. It is well known that the resulting thermal comfort of the occupants will be affected by other parameters, mainly the mean radiant temperature. At a time when the air-conditioned cooling was prevalent in the office, the simulation model was calibrated according to the measured air temperature. Very satisfactory accuracy was achieved, expressed using the coefficient of variation (2.5%). But in the mean radiant temperature, there was a big difference between measurement and simulation. This was due to a large difference in surface temperatures. It was mainly the temperature of the floor (3 K) and the glazing on the window (4 K). Those temperatures were more affected by the airflow in the room. Such inaccuracy (of up to 4 K in mean radiant temperature (MRT)) led to the inaccuracy of 0.5 points in the PMV index estimate. To prevent this, it would be useful to know the airflow image in a detail, even with the temperature distribution. Until the building is in operation, this can be obtained by more complex computer fluid flow simulation (CFD) only. When architects design buildings, the CFD simulation is not usually available for various reasons.

At a time when the ceiling radiant cooling method prevailed in the office, the simulation model ceased to be very accurate in predicting air temperature. The simulation settings

for the convective cooling system stopped fitting after the system change on the radiant cooling system. The accuracy expressed by CV (RMSE) was 3.8% in this case. But the accuracy of the mean radiant temperature simulation increased. The CV (RMSE) parameter decreased from 12% to 6%. The difference between the simulated air temperature around 1 K and the mean radiant temperature around 1 K caused the root-mean-square error of 0.28 points in the PMV index. From this, we conclude that we can more easily achieve agreement in the estimated thermal comfort conditions with ceiling radiant cooling than with air-conditioned cooling.

It should be added that the thermal environment in the office was slightly colder during the measurement than is ideal for the sedentary activity. It was necessary to choose a higher activity and clothing level when calculating PPD and PMV indices. From the evaluation of the measured and simulated values, it was found that with the blinds drawn and no natural shading, overheating of the indoor environment occurs even in buildings that have been designed and constructed as a low-carbon. Indoor temperatures attack the maximum permissible indoor comfort temperatures. In the morning, the thermal comfort was in EIQ Category III, in the afternoon, due to warming, it reached EIQ Category II. It was reached more by simulation and less by measurement. According to the measurement, this was achieved in the opposite way as according to the simulation. But there was still a change from one category to another during the day. The difference has diminished more with the accumulated PPD index statistical evaluation.

These facts encourage further research in the field of adaptive thermal comfort. This was used in non-air-conditioned buildings at first, but in the area of the mild climate, it is possible to use it for the so-called mixed-mode buildings. In mixed-mode buildings, offices are intensely cooled at night by ventilation through the windows. During the day, offices are cooled by low-performance air conditioning. Such a system will need to be set up well by the simulation to avoid the feeling of cold in the morning, as we evaluated in this study. This problem could be further complicated by considering a different internal heat gain from the office equipment. Although this parameter is probably less important for thermal comfort in summer [9]. Several human-behavior predictive models have been developed recently, which we could apply to the Research Centre building in the future [34].

Author Contributions: Conceptualization, R.P. and P.B.; methodology, R.P.; software, R.P.; validation, R.P.; data curation, P.B.; writing—original draft preparation, P.B. and R.P.; writing—review and editing, R.P.; supervision, P.Ď.; project administration, P.Ď.; funding acquisition, P.Ď. All authors have read and agreed to the published version of the manuscript.

Funding: This research was funded by VEGA, grant number 1/0673/20 Theoretical and experimental analysis of energy effective and environmentally friendly building envelopes.

Data Availability Statement: Not applicable.

Conflicts of Interest: The authors declare no conflict of interest.

References

1. D'Ambrosio Alfano, F.R.; Olesen, B.W.; Palella, B.I.; Riccio, G.; Pepe, D. Fifty Years of PMV Model: Reliability, Implementation and Design of Software for Its Calculation. *Atmosphere* **2019**, *11*, 49. [CrossRef]
2. Fanger, P.O. *Thermal Comfort. Analysis and Applications in Environmental Engineering*; Danish Technical Press: Copenhagen, Denmark, 1970.
3. Zhang, H.; Arens, E.; Huizenga, C.; Han, T. Thermal sensation and comfort models for non-uniform and transient environments: Part I: Local sensation of individual body parts. *Build. Environ.* **2010**, *48*, 380–388. [CrossRef]
4. Rijal, H.B.; Humphreys, M.; Nicol, F. Adaptive Thermal Comfort in Japanese Houses during the Summer Season: Behavioral Adaptation and the Effect of Humidity. *Buildings* **2015**, *5*, 2075–5309. [CrossRef]
5. Chen, X.; Gao, L.; Xue, P.; Gu, J.; Liu, J. Investigation of outdoor thermal sensation and comfort evaluation methods in severe cold area. *Sci. Total Environ.* **2020**, *749*, 141520. [CrossRef] [PubMed]
6. Chen, A.; Chang, W.-C.V. Human health and thermal comfort of office workers in Singapore. *Build. Environ.* **2012**, *58*, 172–178. [CrossRef]
7. Heinzerling, D. *Commercial Building Indoor Environmental Quality Evaluation: Methods and Tools*; University of California: Berkley, CA, USA, 2012. Available online: https://escholarship.org/uc/item/2f6562gr (accessed on 22 December 2020).

8. Park, J.; Loftness, V.; Aziz, A. Post-Occupancy Evaluation and IEQ Measurements from 64 Office Buildings: Critical Factors and Thresholds for User Satisfaction on Thermal Quality. *Buildings* **2018**, *8*, 156. [CrossRef]
9. Ponechal, R.; Chabada, M. The Impact of Ventilation and Shading Control on the Result of Summer Overheating Simulation. *Civ. Environ. Eng.* **2021**, *17*, 327–334. [CrossRef]
10. Bueno, A.M.; Xavier, A.A.d.P.; Broday, E.E. Evaluating the Connection between Thermal Comfort and Productivity in Buildings: A Systematic Literature Review. *Buildings* **2021**, *11*, 244. [CrossRef]
11. Fantozzi, F.; Rocca, M. An Extensive Collection of Evaluation Indicators to Assess Occupants' Health and Comfort in Indoor Environment. *Atmosphere* **2020**, *11*, 90. [CrossRef]
12. Christensen, J.E.; Chasapis, K.; Gazovic, L.; Kolarik, J. Indoor Environment and Energy Consumption Optimization Using Field Measurements and Building Energy Simulation. 6th International Building Physics Conference, IBPC 2015. *Energy Procedia* **2015**, *78*, 2118–2123. [CrossRef]
13. Cornaro, C.; Puffioni, V.; Adoo, S.; Rodolfo, M. Dynamic simulation and on-site measurements for energy retrofit of complex historic buildings: Villa Mondragone case study. *J. Build. Eng.* **2016**, *6*, 17–28. [CrossRef]
14. Cornaro, C.; Rossi, S.; Cordiner, S.; Mulone, V.; Ramazzotti, L.; Rinaldi, Z. Energy performance analysis of Stile house at the Solar Decathlon 2015: Lessons learned. *J. Build. Eng.* **2017**, *13*, 11–27. [CrossRef]
15. Coakley, D.; Raftery, P.; Keane, M. A review of methods to match building energy simulation models to measured data. *Renew. Sustain. Energy Rev.* **2014**, *37*, 123–141. [CrossRef]
16. Li, N.; Yang, Z.; Becerik-Gerber, B.; Tang, C.; Checn, N. Why is the reliability of building simulation limited as a tool for evaluating energy conservation measures? *Appl. Energy* **2015**, *159*, 196–205. [CrossRef]
17. Hong, T.; Kim, J.; Jeong, J.; Lee, M.; Ji, C. Automatic calibration model of a building energy simulation using optimization algorithm. *Energy Procedia* **2017**, *105*, 3698–3704. [CrossRef]
18. Schünemann, C.; Schiela, D.; Ortlepp, R. Guidelines to Calibrate a Multi-Residential Building Simulation Model Addressing Overheating Evaluation and Residents' Influence. *Buildings* **2021**, *11*, 242. [CrossRef]
19. Zweifel, G. Simulation of displacement ventilation and radiation cooling with DOE2. *ASHRAE Trans.* **1993**, *99*, 548–555.
20. Paliouras, P.; Matzaflaras, N.; Peuhkuri, R.H.; Kolarik, J. Using Measured Indoor Environment Parameters for Calibration of Building Simulation Model- A Passive House Case Study. *Energy Procedia* **2015**, *78*, 1227–1232. [CrossRef]
21. Ricciu, R.; Galatioto, A.; Desogus, G.; Besalduch, L.A. Uncertainty in the evaluation of the Predicted Mean Vote index using Monte Carlo analysis. *J. Environ. Manag.* **2018**, *223*, 16–22. [CrossRef]
22. D'Ambrosio Alfano, F.R.; Palella, B.I.; Riccio, G. The role of measurement accuracy on the thermal environment assessment by means of PMV index. *Build. Environ.* **2011**, *46*, 1361–1369. [CrossRef]
23. CEN. *EN Standard 16798-1:2019*; Energy Performance of Buildings-Ventilation for Buildings-Part 1: Indoor Environmental Input Parameters for Design and Assessment of Energy Performance of Buildings Addressing Indoor Air Quality, Thermal Environment, Lighting and Acous. European Committee for Standardization: Brussels, Belgium, 2019.
24. Available online: https://passiv.de/de/02_informationen/02_qualitaetsanforderungen/02_qualitaetsanforderungen.htm (accessed on 2 February 2022).
25. Dantec Dynamics. Available online: https://www.dantecdynamics.com/comfortsense (accessed on 3 December 2019).
26. CEN. *EN Standard 13182:2002*; Ventilation for Buildings-Instrumentation Requirements for Air Velocity Measurements in Ventilated Spaces. European Committee for Standardization: Brussels, Belgium, 2002.
27. *ISO 7726:1998*; Ergonomics of the Thermal Environment. Instruments for Measuring Physical Quantities. International Organization for Standardization: Geneva, Switzerland, 1998.
28. *ISO 7730:2005*; Ergonomics of the Thermal Environment—Analytical Determination and Interpretation of Thermal Comfort Using Calculation of the PMV and PPD Indices and Local Thermal Comfort Criteria. International Organization for Standardization: Geneva, Switzerland, 2005.
29. Juras, P.; Jurasova, D. Outdoor Climate Change Analysis in University Campus: Case Study with Heat-Air-Moisture Simulation. *Civ. Environ. Eng.* **2020**, *16*, 370–378. [CrossRef]
30. Hand, W.J. *The ESP-r Cookbook: Strategies for Deploying Virtual Representations of the Buil Environment*; Energy Systems Research Unit, Department of Mechanical Engineering University of Strathclyde: Glasgow, UK, 2008; 256p, Available online: https://labeee.ufsc.br/sites/default/files/disciplinas/ECV4202_ESP-r_cookbook_sep2008.pdf (accessed on 21 December 2020).
31. Fisher, D.E.; Pedersen, C.O. Convective heat transfer in building energy and thermal load calculations. *ASHRAE Trans.* **1997**, *103*, 137–148.
32. Tartarini, F.; Schiavon, S.; Cheung, T.; Hoyt, T. CBE Thermal Comfort Tool: Online tool for thermal comfort calculations and visualizations. *SoftwareX* **2020**, *12*, 100563. [CrossRef]
33. Liu, J.; Foged, I.W.; Moeslund, T.B. Clothing Insulation Rate and Metabolic Rate Estimation for Individual Thermal Comfort Assessment in Real Life. *Sensors* **2022**, *22*, 619. [CrossRef]
34. Yi, H. Visualized Co-Simulation of Adaptive Human Behavior and Dynamic Building Performance: An Agent-Based Model (ABM) and Artificial Intelligence (AI) Approach for Smart Architectural Design. *Sustainability* **2020**, *12*, 6672. [CrossRef]